RSC Applied Polymers

ROYAL SOCIETY OF CHEMISTRY

PAPER

View Article Online
View Journal

Cite this: DOI: 10.1039/d5lp00321k

Model-based optimization of properties of post-consumer recycled PP/PE blends *via* compatibilization

Sixtus O. Nzeh, *[a] David O. Kazmer,[a] Margaret J. SobkowiczKline, [a] Thao D. Nguyen[b] and David C. Elbert [b]

The reuse of post-consumer recycled polypropylene (rPP) is limited by poor processability, immiscibility with polyethylene (PE), and reduced mechanical properties. This work applies compatibilization strategies and regression-based optimization to improve the performance of a monolayer cast-film of a commercial recyclate containing ~55 wt% PP and ~45 wt% HDPE. Three compatibilizers were examined: maleic anhydride-grafted-polyethylene (PEMA), maleic anhydride-grafted-polypropylene (PPMA), and an ethylene–propylene copolymer (EPB). Tensile testing in the machine (MD) and transverse (TD) directions, FTIR, and SEM were combined with multiple regression to guide blend formulation. PEMA and PPMA exhibited quadratic effects on yield stress with optima near 8–11 wt%, whereas EPB showed a positive linear effect on modulus. At practical loadings, model coefficients correspond to gains of ~6.1 MPa and ~4.2 MPa in yield stress for 10 wt% PEMA and PPMA respectively, and ~+5 MPa and +170 MPa in yield stress and modulus respectively for 20 wt% EPB. Two model-guided blends: (i) single-objective optimization (based on PEMA/EPB) and (ii) multiple objective optimization (based on PEMA/PPMA/EPB), produced smoother films and improved stiffness–ductility balance relative to the uncompatibilized recyclate. Single-objective optimization improved elongation by 3776% (MD) and 1371% (TD), with strength gains of up to 448%. Multiple-objective optimization incorporating 2% PPMA achieved the best balance, combining 1686% higher elongation (TD) with 491% higher yield stress and 240% higher stiffness SEM indicated reduced voiding and more cohesive fracture surfaces; FTIR remained consistent with physical interfacial anchoring/bridging rather than new covalent bonding. These results highlight a materials design pathway to enable reliable, high-performance use of recycled PP/PE blends in film and packaging applications.

Received 11th October 2025,
Accepted 1st March 2026

DOI: 10.1039/d5lp00321k

rsc.li/rscapplpolym

1. Introduction

Polyolefins are amongst the widely used thermoplastics that can be recycled and reused. The global production and consumption of polyolefins are increasing rapidly due to their versatility across diverse applications. In 2024, the polyolefin market was valued at approximately USD 262.71 billion and is projected to reach USD 357.39 billion by 2030, growing at a compound annual growth rate (CAGR) of 5.4% between 2025 and 2030.[1] Among polyolefins, polyethylene (PE) dominated the market, accounting for 37.66% of the total revenue in 2024, followed by polypropylene (PP) at 27%.[2,3] Despite some known commercial pathways, polyolefins exhibit alarmingly low recycling rates.[4] According to several reports,[5,6] only 10% of high-density polyethylene (HDPE) is currently recycled, while 82% is landfilled and 8% incinerated. The situation is more severe for polypropylene (PP), with just 3% recycled, 88% landfilled, and 9% combusted.

The low recycling rates of polyolefins are primarily attributed to the challenges associated with sorting plastics waste into single-polymer streams and the cost-intensive nature of recycling processes.[7–12] Municipal plastic waste, especially from densely populated urban areas, typically consists of heterogeneous mixtures, including polyethylenes (PE), polypropylenes (PP), styrenics, polyvinyl chloride (PVC), and polyethylene terephthalate (PET), and in many cases effective separation is extremely difficult and economically nonviable.[7,8,13] Among these, the separation of PE and PP remains particularly problematic due to their similar physical and chemical properties, such as density and melting points, which often fall within overlapping ranges.[14] This similarity results in cross-contamination, undermining the quality and performance of the recycled output.[15,16]

[a]*Department of Plastics Engineering, University of Massachusetts Lowell, Lowell, Massachusetts 01854, USA. E-mail: sixtusdika@gmail.com; Tel: +1(978)-221-0432*
[b]*Department of Mechanical Engineering, Johns Hopkins University, Baltimore, Maryland, USA*

Consequently, post-consumer recycled (PCR) polyolefins frequently exhibit inferior mechanical properties as well as reduced chemical and thermal resistance, largely due to the incompatibility between the polymers and contaminants, and the mechanical stresses imposed during reprocessing.[17–24] This variability is particularly problematic in film extrusion applications, where melt strength and flow stability are essential for producing thin, uniform films. Processing recycled PP contaminated by PE or recycled PE contaminated by PP into cast films often leads to melt bifurcation, melt fracture, and phase separation during crystallization,[25] all of which severely compromise product quality. These processing instabilities are compounded by the interfacial tension and lack of adhesion (incompatibility) between the PE and PP phases in the melt.[26,27]

To address these challenges, this research investigates compatibilization strategies to improve interfacial adhesion, reduce phase separation, and stabilize melt flow in recycled polypropylene/polyethylene blends. Previous studies have demonstrated the promise of compatibilizers such as olefin block copolymers[28–35] and grafted polyolefins,[36–39] but most evaluations are limited to compression and injection molded specimens, which do not fully replicate the processing dynamics of film extrusion-based applications.

Meanwhile, the choice of compatibilizer is strongly dependent on the nature of the blend system. For immiscible PE/PP blends, polyolefin elastomers such as ethylene–propylene rubber (EPR) and ethylene–propylene–diene terpolymer (EPDM) have received considerable attention. The propylene units in EPR/EPDM can insert into the PP phase, while the ethylene units align with the PE phase, thereby improving compatibility and mechanical performance. For example, D'Orazio *et al.*[29] reported that adding 15 wt% EPR to a PP/HDPE (75/25) blend increased impact strength by 2100% and tensile strength by 34% compared to the neat blend. Similarly, Choudhary *et al.*[30] found that introducing 20 wt% EPDM to a 90/10 iPP/HDPE blend enhanced impact strength by 620% relative to the uncompatibilized system.

Grafted polyolefins such as maleic anhydride-grafted polyethylene (PEMA) and polypropylene (PPMA) have also been widely explored for PP/PE systems.[38–41] PEMA interacts preferentially with the PE phase, while PPMA is miscible with the PP phase, enabling improved interfacial adhesion. The maleic anhydride units are thought to engage in free radical reactions that can result in grafting between the immiscible phases, thereby reinforcing the interfaces. However, this reactive system is more commonly employed for polyolefin blends with more polar polymers such as nylon or PET.[42–46] Colbeaux *et al.*[39] demonstrated that a ternary compatibilizer system of PPMA, PEMA, and a coupling agent (dodecane diamine) increased elongation at break by 800% in a 70/30 PP/HDPE blend, owing to covalent linkages between the anhydride and amine groups. Similarly, Tselios *et al.*[38] used PPMA and polyethylene-*co*-vinyl alcohol (EVAL) as compatibilizers for a 75/25 iPP/LDPE blend, reporting increases of 47% in elongation at break, 22% in tensile strength, and 44% in impact strength compared to the uncompatibilized blend. Marco *et al.*[36] showed that the incorporation of PP-*g*-MA into a 70/30 iPP/PA6 blend led to a progressive increase in shear viscosity with compatibilizer content, with interfacial adhesion and mechanical properties improving up to 10 wt% loading. More recently, Lin *et al.*[28] reported that the addition of 7 wt% maleic anhydride-grafted polyethylene-octene copolymer (POE-*g*-MAH) to PA6/olefin block copolymer (OBC) blends increased melt viscosity, storage modulus (G'), and loss modulus (G''), while impact strength improved by 194% compared to neat PA6.

In contrast to prior studies, which frequently relied on indirect measures or model polymer systems, the present work focuses on real post-consumer recycled feedstock rather than virgin polymers or controlled model blends. Compatibilization performance was evaluated directly through cast film extrusion rather than compression molded samples, a process-sensitive approach in which extrusion stability and tensile properties were used as sensitive indicators of interfacial interaction and phase dispersion. Furthermore, this study systematically investigates the performance of three structurally distinct polyolefin-based compatibilizers, each with different interaction mechanisms and explores binary and ternary compatibilizer combinations to identify optimal formulations for improving morphology, mechanical integrity, and processability of recycled polypropylene films.

2. Materials and methods

2.1 Materials

The primary polymer of interest used in this study was a post-consumer recycled polypropylene blend, referred to as rPP2. According to the safety data sheet (SDS), the material is identified as ITRA-PP-REPRO-Car Grade, manufactured by Intramex (Monterrey, Nuevo León, Mexico) and supplied in bulk (100-pound drums) by Geon Performance Solutions (Avon Lake, OH, USA). As described in a prior article[47] focused on characterization of recycled polypropylenes, rPP2 consists of approximately 55 wt% isotactic polypropylene (iPP) and 45 wt% high-density polyethylene (HDPE). rPP2 is a pre-compounded blend of rPP and rPE in which the fraction of rPE was varied to deliver a targeted melt flow index. It should be noted that no characterization of chemical impurities (such as additives) was conducted, but it is likely that some minority contaminants are likely present since it is a real post-consumer recycled grade.

Three different polyolefin-based compatibilizers were investigated with respect to their blending and enhancement of the rPP2 in the cast film extrusion process:

- PPMA: a maleic anhydride grafted polypropylene (Orevac CA100) with ~1 wt% MAH, produced by SK Functional Polymer (Courbevoie, France). The melt flow rate is 10 g per 10 min at 190 °C per 0.325 kg, and melting point of 167 °C. The material was used as received.
- PEMA: maleic anhydride-grafted linear low-density polyethylene (LLDPE; Bynel™ 41E710, Dow Chemical Company, Midland, MI, USA) containing approximately 1 wt% MAH. The

material has a melt flow rate of 2.7 g per 10 min (190 °C per 2.16 kg) and a melting point of 115 °C and was used as received.

• EPB: ethylene–propylene copolymer (Pro-fax™ 7823) described in its SDS as a propylene copolymer (1-propene polymer with ethene). The material contains >99.5 wt% of the copolymer, with the remainder comprising standard additives and stabilizers. It was produced by LyondellBasell Industries (Houston, TX, USA) and supplied by Geon Performance Solutions (Avon Lake, OH, USA). The copolymer was used as received.

The three compatibilizers were carefully selected to represent distinct compatibilization material strategies for improving interfacial adhesion in immiscible polyolefin-based blends. PPMA consists of polypropylene grafted with maleic anhydride (~1 wt% MAH), was selected due to its polypropylene backbone, which promotes compatibility with the PP phase, while the maleic anhydride functionality can interact with polar species commonly present in post-consumer recycled materials like our rPP2. This compatibilizer is designed to interact with polar and nonpolar domains in polyolefin blends through interfacial anchoring mechanisms.[38,48] PEMA, consisting of maleic anhydride-grafted linear low-density polyethylene (LLDPE-*g*-MAH), was chosen to provide compatibility with the PE-rich phase in rPP2, while simultaneously introducing polar functional groups at the PP/PE interface. The LLDPE backbone also imparts elastomeric characteristics that can enhance stress transfer and toughness.[49] The third compatibilizer investigated in this study is a copolymer of ethylene and propylene. The EPB copolymer contains ethylene and propylene blocks randomly distributed. The third compatibilizer, a PE–PP copolymer, was selected to represent a non-polar, architecture-based compatibilization approach, as its molecular structure contains segments compatible with both PP and PE phases, enabling interfacial bridging without the use of reactive functional groups. All compatibilizers are industrially available and have been widely reported in the literature for improving mechanical performance in polyolefin blend systems.[31–35,38,48–50]

2.2 Extrusion of cast film samples

Monolayer cast film samples were produced using a Dr Collin Teach-Line coextrusion system (Dr Collin GmbH, Maitenbeth, Germany). While the equipment comprises five single-screw extruders and a coextrusion feedblock, only the central core extruder (Extruder #3) was employed for monolayer film production in this study (see SI, Fig. S1 for a schematic of the extrusion line). The selected extruder features a screw with a length-to-diameter (L/D) ratio of 30 : 1 and 28 turns. The feedblock is designed so that extruder #3 exclusively supplies the central core layer. The extrusion line includes a coat-hanger die designed to produce a film with an initial thickness of 0.5 mm and a width of 246 mm. The film was subsequently drawn down through a chill roll stack to a target film thickness of approximately 250 μm. The temperature profile across the extruder zones was set as follows: 150 °C (feed zone), 180 °C (transition zone), and 200 °C (metering zone). The feedblock and die were both maintained at 230 °C to ensure uniform flow and interfacial stability. A constant screw speed of 60 RPM was maintained throughout processing to ensure consistency with typical residence time.

The design of experiments (DOE) is summarized in Table 1, which details a one-factor-at-a-time (OFAT) approach used to evaluate the effects of three compatibilizers: PEMA, PPMA, and EPB, on film properties. This approach with runs 1 to 10 enabled estimations of the main and quadratic effects of each compatibilizer while minimizing direct confounding from simultaneously varying factors. Although OFAT does not provide uniform coverage of the mixture design space or fully accounts for possible higher-order interactions among components, it was selected here to isolate the primary influence of each compatibilizer under controlled processing conditions. More comprehensive mixture designs (*e.g.*, simplex-centroid or definitive screening) could be employed in future work to capture potential synergistic effects more systematically. Further, runs 11 and 12 augment the OFAT design to investigate the potential interaction effects between PEMA and PPMA. Table 1 also features the optimization runs predicted and performed after processing of the initial experimental runs 1–12, the characterization of the film extrudates, and statistical modeling of the film properties. All formulations were prepared as dry blends (by weight%) of the base matrix (rPP2) with varying weight percentages of each compatibilizer, according to the DOE specifications. The dry blends were directly fed into the extruder hopper without prior melt compounding. This approach was adopted to (i) ensure no additional heat cycle was added to the rPP2 prior to film extrusion and (ii) replicate a typical industrial approach.

2.3 Mechanical characterization

The tensile properties of all film specimens were evaluated using an MTS universal testing machine (Model C43, Eden Prairie, MN, USA) equipped with a 2 kN load cell. For each of the eleven experimental formulations, including optimization runs, five replicate specimens were prepared for both the

Table 1 Design of experiments

S/N	Run name	Run description
1	rPP2-CTRL	No compatibilizer (control sample)
2	rPP2-PPMA-5	95%rPP2 + 5% of PPMA
3	rPP2-PPMA-10	90%rPP2 + 10% of PPMA
4	rPP2-PPMA-20	80%rPP2 + 20% of PPMA
5	rPP2-PEMA-5	95%rPP2 + 5% of PEMA
6	rPP2-PEMA-10	90%rPP2 + 10% of PEMA
7	rPP2-PEMA-20	80%rPP2 + 20% of PEMA
8	rPP2-EPB-5	95%rPP2 + 5% of EPB
9	rPP2-EPB-10	90%rPP2 + 10% of EPB
10	rPP2-EPB-20	80%rPP2 + 20% of EPB
11	rPP2-PPMA/PEMA-2.5/2.5	95%rPP2 + 2.5%PPMA + 2.5%PEMA
12	rPP2-PPMA-PEMA-5	90%rPP2 + 5%PPMA + 5%PEMA
OPT1	Single objective optim (SOO)	71%rPP2 + 9%PEMA + 20% EPB
OPT2	Multiple objective optim (MOO)	70%rPP2 + 8%PEMA + 20% EPB + 2%PPMA

machine direction (MD) and the transverse direction (TD) in accordance with ASTM D882-18.[51] Tensile specimens were prepared by cutting 12.7 mm (0.5 inch) wide strips using a precision strip cutter. The film thickness, ranging from 200 to 250 μm, was measured for each specimen and entered into the testing software prior to testing. A grip-to-grip separation of 50.8 mm and a crosshead speed of 101.6 mm min^{-1} were used for all tests. To minimize stress concentrations at the gripping points, Teflon tape was applied to the clamp surfaces. Once specimens were mounted, the crosshead was adjusted to remove slack, and both load and displacement channels were zeroed before test initiation.

All specimens were tested to fracture, tensile properties were recorded, and multiple regression analysis was performed using the following performance measures: (1) elastic modulus, calculated as the slope of the initial linear region of the stress–strain curve, within the strain range of 0.05% to 0.25%, (2) yield strength (yield stress), and (3) elongation at break. A complete dataset of tensile test results is provided in supplemental materials.

2.4 Statistical analysis

Statistical analysis was conducted to model and optimize the mechanical performance of the extruded film blends as a function of rPP2 material and weight fractions of the three compatibilizers: maleic anhydride-grafted polyethylene (PEMA, x_1), maleic anhydride-grafted polypropylene (PPMA, x_2), and ethylene–propylene copolymer (EPB, x_3). Multiple regression analyses were performed to estimate the influence of each compatibilizer on three key mechanical responses (elastic modulus, yield strength, and elongation at break) using data from 120 observations from experimental runs 1 to 12. To model the effect of anisotropy on the film properties, the film orientation was included as a factor MD which was set to 1 for specimens in the machine (extrusion) direction (MD) and 0 for specimens in the transverse direction (TD).

Outlier analysis was recursively performed in which the multiple regression analyses were performed for each response and any observations with a residual error greater than two standard errors (corresponding roughly to a confidence interval of 95%) were removed. Additional iterations of multiple regression analyses and outlier identification were performed until no additional outliers were observed or a maximum of 20 outliers (corresponding to 16% of the size of the data set) were obtained. This analysis methodology ensured that a super majority of the observations were included to provide a model representative of the global behavior even if the fitting statistics could be improved by removing additional outliers.† In further detail, the resulting regression model coefficients and associated statistical measures are later presented in Tables

†In more detail, it was found that unlimited recursive outlier removal could result in less than half of the 120 observations being included in the model. The resulting models demonstrated high coefficients of determination, R^2, on the order of 0.95 or greater but excluded entire sets of material blends and so were understood to not be representative of the global behavior.

Table 2 Multiple regression model for yield stress across 100 observations. Error degrees of freedom: 86, RMSE: 1.51, *R*-squared 0.853, adjusted *R*-squared: 0.832

	Estimate (β)	Standard error	tStat	*P*-Value
Yield stress (MPa)				
β_0, intercept	2.693	0.4857	5.545	3.10×10^{-07}
β_1, PEMA	61.33	13.69	4.479	2.26×10^{-5}
β_2, PPMA	42.31	13.69	3.0903	0.002685
β_3, EPB	26.18	4.65	5.629	2.17×10^{-7}
β_4, MD	5.360	0.7118	7.531	4.41×10^{-11}
β_5, PEMA*PPMA	−698.3	281.9	−2.478	1.52×10^{-2}
β_6, PEMA*MD	−7.233	18.73	−0.3862	7.00×10^{-1}
β_7, PPMA*MD	39.96	19.64	2.0346	4.49×10^{-2}
β_8, EPB*MD	2.554	6.372	0.4009	6.89×10^{-1}
β_9, $PEMA^2$	−290.1	66.68	−4.350	3.68×10^{-5}
β_{10}, $PPMA^2$	−257	66.68	−3.854	2.22×10^{-4}
β_{11}, $PEMA^2$*MD	−17.36	93.54	−0.1856	8.53×10^{-1}
β_{12}, $PPMA^2$*MD	−188.4	96.069	−1.961	5.31×10^{-2}

Table 3 Multiple regression model for elongation at break (% strain) across 111 observations. Error degrees of freedom: 97, RMSE: 159, *R*-squared 0.74, adjusted *R*-squared: 0.708

	Estimate (β)	Standard error	tStat	*P*-Value
Elongation at break				
β_0, intercept	5.164	50.74	0.1018	0.9191
β_1, PEMA	89.54	1437	0.06232	0.9504
β_2, PPMA	−7.0169	1437	−0.00488	0.9961
β_3, EPB	104.7	459.2	0.2279	0.8202
β_4, MD	85.84	72.003	1.192	0.2361
β_5, PEMA*PPMA	−162.3	29 259	−0.00555	0.9956
β_6, PEMA*MD	7021	1992	3.524	0.000648
β_7, PPMA*MD	5008	1910	2.622	0.01014
β_8, EPB*MD	4461	647.2	6.893	5.34×10^{-10}
β_9, $PEMA^2$	−520.09	7013	−0.07416	0.9410
β_{10}, $PPMA^2$	2.258	7013	0.000322	0.9997
β_{11}, $PEMA^2$*MD	−33 669	9861	−3.414	0.000931
β_{12}, $PPMA^2$*MD	−24 648	9365	−2.632	0.009863

Table 4 Multiple regression model for modulus across 101 observations. Error degrees of freedom: 87, RMSE: 69.1, *R*-squared 0.729, adjusted *R*-squared: 0.693

	Estimate (β)	Standard error	tStat	*P*-Value
Modulus (MPa)				
β_0, intercept	455.4	32.44	14.038	3.51×10^{-24}
β_1, PEMA	413.5	761.8	0.5427	0.5887
β_2, PPMA	105.4	757.9	0.1390	0.8898
β_3, EPB	871.4	252.5	3.3451	0.000861
β_4, MD	28.86	38.95	0.7409	0.4607
β_5, PEMA*PPMA	−5795	12 862	−0.4506	0.6534
β_6, PEMA*MD	598.9	928.2	0.6452	0.5205
β_7, PPMA*MD	475.5	910.5	0.5223	0.6028
β_8, EPB*MD	−382.6	318.9	−1.2	0.2334
β_9, $PEMA^2$	−5270	3461	−1.522	0.1315
β_{10}, $PPMA^2$	−9217	3465	−2.660	0.009291
β_{11}, $PEMA^2$*MD	−2559	4387	−0.5833	0.5612
β_{12}, $PPMA^2$*MD	4577	4348	1.0526	0.2954

2–4. The regression coefficients (β values) quantify the magnitude and direction of influence each predictor variable (*i.e.* the compatibilizers) exert on the dependent variables. These coefficients estimate the expected change in response per unit increase in compatibilizer content, assuming all other variables remain constant.

2.5 Single and multiple objective optimization

Optimization in materials design involves formulating objective functions that represent desired material properties and then applying modeling routines to identify material combinations that maximize performance subject to practical constraints. The optimization framework adopted here builds on established principles of robust design and stochastic optimization, which emphasize not only maximizing nominal performance but also mitigating the effects of variability inherent in recycled materials. Similar approaches have been applied in polymer blend and process design to account for nonlinear and interacting factors,[52] as well as in broader engineering design contexts where robust trade-offs are essential in model-based optimization.[53]

In this work, optimization was conducted in MATLAB R2023b using the fmincon function, which implements a constrained nonlinear programming approach based on interior point methods.[54] The optimization variables corresponded to the weight fractions of the three compatibilizers: maleic anhydride grafted polyethylene (PEMA, x_1), maleic anhydride grafted polypropylene (PPMA, x_2), and ethylene–propylene copolymer (EPB, x_3) with bounds set between 0 and 0.20 (20 wt%).

Following the statistical model from previous section, both single and multiple objective functions, G_1 and G_2, were respectively maximized based on the modeled response functions. For the single-objective optimization, the function to maximize was the predicted elongation at break in the transverse direction (TD) since that one property dominates the performance of the film in actual application. This objective function is:

$$\max_{0\le x_i\le 0.2} G_1 = -\text{Elongation}_{\text{TD}}(x_1, x_2, x_3)$$

Here, the negated value of elongation was evaluated since fmincon solves minimization problems.

The multi-objective optimization (MOO) seeks to maximize the joint performance considering the competing requirements of stiffness, strength, and ductility as normalized using a scalarization approach. Here, a desirability-based formulation was employed in which normalized predictions of modulus, yield strength, and elongation at break were combined through their geometric mean according to the multiple objective function G_2 as:

$$\max_{0\le x_i\le 0.2} G_2 = -\prod_{i=1}^{3}\prod_{j\in\{\text{MD,TD}\}} \frac{\hat{y}_{i,j}(x_1, x_2, x_3)}{\bar{y}_{i,j}}$$

Here, $\hat{y}_{i,j}$ are the regression model predictions for the i-th performance attribute (modulus, yield strength, and elongation coefficients presented in Tables 2–4) in the j-th machine directions and transverse directions while $\bar{y}_{i,j}$ represent their respective dataset means. This formulation reflects the principle of multi-objective trade-off optimization, where Pareto-efficient solutions must balance conflicting performance criteria. By normalizing each performance attribute relative to the dataset mean, it is understood that the multiple objective function still emphasizes the important behavior of elongation since that fraction tends to dominate the performance of the material in application. The optimization outcomes were used to create new material formulations as listed in Table 1 and subsequently produced and tested.

2.6 Scanning electron microscopy (SEM)

The morphology of all specimens was examined in the machine direction (MD) using a field emission scanning electron microscope (FE-SEM) (JEOL JSM-7401F, Peabody, MA, USA). Film samples were first cryo-fractured under liquid nitrogen to preserve microstructural features during fracture. The fractured surfaces were then sputter-coated with gold for 180 seconds to ensure adequate electrical conductivity during imaging.

SEM imaging was conducted at an accelerating voltage of 5.0 kV and a working distance of 8.0 mm. The MD orientation was selected specifically to capture morphology developed under shear and elongational flow conditions during film extrusion. This directional analysis enabled evaluation of how each compatibilizer type and concentration influenced the phase dispersion, interfacial interaction, and overall microstructure of the recycled polypropylene (rPP2) matrix under processing conditions.

2.7 Fourier-transform infrared spectroscopy (FTIR)

Fourier-transform infrared (FTIR) spectroscopy was conducted to identify functional group interactions and assess chemical changes associated with compatibilizer incorporation into the rPP2 matrix. Extruded film specimens from blends containing 10 wt% of each compatibilizer (PPMA, PEMA, and EPB) were analyzed, along with specimens from the single-objective optimized formulation and the multi-objective optimized formulation. All FTIR measurements were performed in attenuated total reflectance (ATR) mode using Nicolet iS50 FTIR spectrometer (Thermo Fisher Scientific, Waltham, MA, USA) equipped with an attenuated total reflectance (ATR) accessory. Spectra were collected over the range of 4000–400 cm^{-1} at a spectral resolution of 4 cm^{-1}, with 64 scans averaged per sample to enhance signal-to-noise ratio.[55] For reference spectra, individual pellets of rPP2 and each compatibilizer were individually characterized. Each of these materials were deformed from individual pellets into flat films using a Carver press (Model 4389, Wabash, IN, USA) at room temperature (25 °C) and with a contact force of 100 kN. These films were scanned using the same ATR-FTIR conditions to facilitate direct comparison and interpretation of the blended materials. Background spectra were collected prior to each measurement to ensure accuracy and to account for environmental or instrumental artifacts.

All spectra were baseline-corrected and normalized to the highest and consistent intensity peak at 2915 cm^{-1} representing the methylene stretch common to all polyolefins prior to analysis using a Matlab code. The resulting spectra were used to identify characteristic peaks corresponding to functional groups and to detect potential interactions or shifts in absorption bands associated with compatibilization. The Matlab code and all the full FTIR spectra are provided in the SI.

2.8 Thermal characterization (differential scanning calorimetry)

Differential scanning calorimetry (DSC) was performed on the rPP2 film, as well as on the single-objective optimization (SOO) and multi-objective optimization (MOO) film samples. For each material specimen, DSC was conducted in N_2 environment using a first heating, cooling, and second heating cycle, with a temperature ramp rate of 10 °C per minute in accordance with ASTM D3418. Measurements were carried out using a Differential Scanning Calorimeter 3+ (Mettler Toledo, Columbus, OH).

3. Results and discussion

3.1 Fourier transform infrared (FTIR) analysis

FTIR spectroscopy was employed to characterize the chemical interactions and confirm the incorporation of compatibilizers into the recycled polypropylene (rPP2) matrix. Fig. 1 presents the average normalized FTIR spectra for neat rPP2, the three compatibilizers (EPB, PEMA, PPMA), their 10 wt% blends with rPP2, as well as the single- and multiple-objective optimized formulations.

All spectra exhibited strong absorption bands between 2800 and 3000 cm^{-1}, corresponding to the asymmetric and symmetric stretching vibrations of $-CH_2-$ and $-CH_3-$ groups, characteristic of polyolefin-based materials. Characteristic polypropylene and polyethylene absorptions were evident in the fingerprint region of all spectra. Distinct peaks at approximately 1378 cm^{-1} and 1168 cm^{-1}, corresponding to $-CH_3$ bending and wagging vibrations characteristic of polypropylene, were observed in all polypropylene-containing materials. Additionally, a peak at 1465 cm^{-1}, assigned to the bending mode of $-CH_2$ groups present in both polyethylene and polypropylene, appeared in all spectra. A further notable feature was the band near 720 cm^{-1}, attributed to $-CH_2$ rocking typical of polyethylene, which was present in all polyethylene-containing samples. Collectively, these observations confirm that the fingerprint region of the examined blends is dominated by polyolefin-specific vibrational signature.

A pronounced absorption band centered at approximately 1645 cm^{-1} was observed in the neat rPP2 spectrum and persisted in all rPP2-based blends. This band was absent in the spectra of the neat compatibilizers (EPB, PPMA, PEMA), confirming that it originates from the recycled polypropylene (rPP2) matrix. The 1645 cm^{-1} band intensity decreased systematically with the reduction of rPP2 content in the blends, indicating a proportional relationship to the rPP2 fraction. This trend strongly indicates that the source of the absorption is intrinsic to rPP2 rather than arising from compatibilizer chemistry. Spectrally, the 1645 cm^{-1} wavenumber is typically attribu-

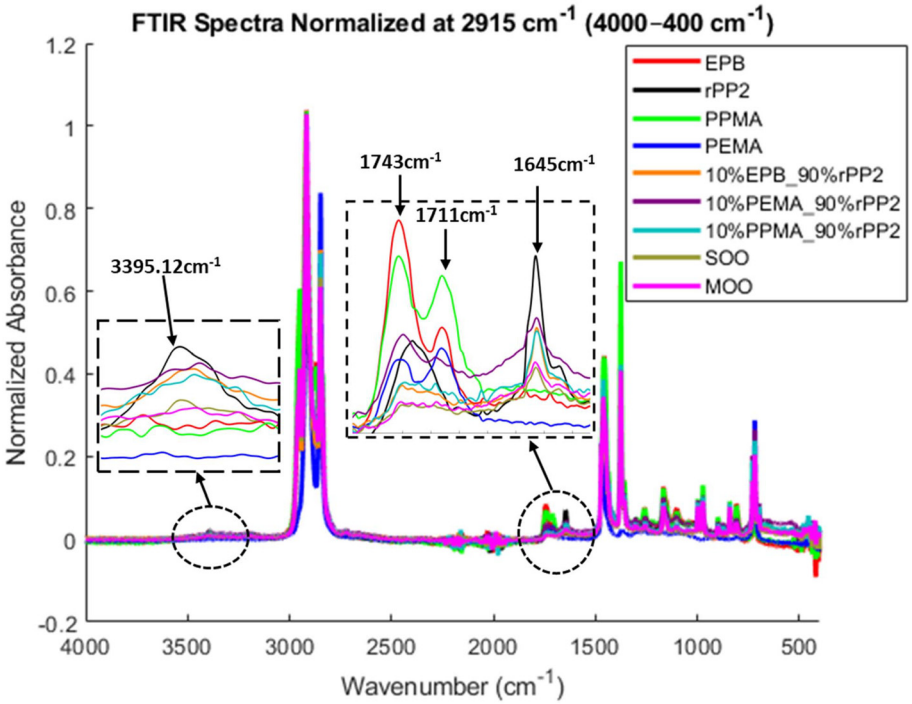

Fig. 1 FTIR Spectra of rPP2, compatibilizers, and blends with absorbance normalize to 2915 cm^{-1}!

ted to the secondary amine bend (1650–1550 cm^{-1}).[56] The persistence of this feature in all blends, combined with its proportional attenuation as rPP2 content decreases, suggests it represents a matrix-specific chemical signature linked to the recycled origin of the polypropylene. Compatibilizer addition, whether maleic anhydride-grafted (PPMA, PEMA) or non-maleated (EPB), did not chemically consume or significantly shift this functional group, as evidenced by the retained peak position and proportional intensity change.

Moving to the carbonyl region (1800–1650 cm^{-1}), two distinct absorptions were noted. At 1711 cm^{-1}, PPMA and PEMA displayed clear peaks, whereas EPB showed only a weak shoulder. This band is characteristic of C=O stretching in maleic anhydride or ester linkages, confirming the presence of grafted maleic anhydride functionalities in PPMA and PEMA and suggesting the presence of a small amount of C=O in EPB. At 1743 cm^{-1}, all spectra exhibited peaks of varying intensities. EPB showed the highest peak intensity, followed by PPMA, the 10 wt% PEMA blend, neat rPP2, and neat PEMA. In contrast, the 10 wt% PPMA and EPB blends presented only a weak, broad feature, while both optimized blends (single- and multiple-objective) lacked any well-defined peak. These differences in intensity and sharpness indicate variations in carbonyl-containing species content and/or their molecular environment, with the absence of a distinct peak in the optimized blends indicating interactions or compatibilization that alter the detectability of carbonyls in ATR-FTIR spectra.

In addition, a weak, broad band near 3395 cm^{-1} was present even in neat rPP2, likely originating from terminal hydroxyl groups, absorbed moisture, or oxidation products formed during previous processing cycles. Its persistence across all blends suggests that this feature is related to the base recycled material rather than the compatibilizers. It is important to note that, no new peaks or significant absorption bands beyond the expected polyolefin C–H vibrations were detected across all samples, indicating that compatibilization occurred primarily through physical interactions and improved miscibility rather than the formation of new covalent bonds. Collectively, the FTIR analysis provides some evidence of effective compatibilizer incorporation at the molecular level, consistent with improved film uniformity and mechanical performance discussed below.

3.2 Visual characteristics of film samples

To provide qualitative insight into how compatibilizer content affects processing behavior and film formation, a high-resolution camera was mounted downstream of the coat hanger die during extrusion. Images were captured for all the runs, including both single and multiple optimization runs corresponding to the model-predicted optima. Representative images are provided in Fig. 2. At low compatibilizer levels (0% and 5%), films exhibited pronounced surface irregularities, sharkskin appearance, and occasional melt fracture with holes that are indicative of incomplete phase dispersion and weak interfacial adhesion between the polypropylene (~55%) and polyethylene (~45%) phases in the recycled rPP2 matrix.

As compatibilizer loading increased to intermediate levels (10%), significant improvements in film stability were observed. Surface smoothness greatly improved but some draw resonance and waviness remained, particularly for formulations with EPB. This behavior is attributed to the elastomeric nature of EPB and its interaction with the HDPE-rich fraction of rPP2 (45% HDPE), where differences in crystallinity and melt elasticity between EPB and HDPE can lead to localized flow instabilities during extrusion and result in minor residual surface waviness. When the compatibilizer loading increased to 20%, the extruded films containing high levels of PEMA and PPMA exhibited numerous holes and poor mechanical integrity. This behavior indicates that excessive compatibilizer incorporation into the rPP2 matrix can lead to interfacial weakening. In contrast, EPB at 20% loading produced films with minimal visible holes and improved strength compared to its 10% counterpart, indicating that EPB effectively promotes interfacial bridging between the PP and PE phases within the recycled matrix. This result is also consistent with the findings of Tselios *et al.*,[38] who demonstrated that in PP/LDPE blends compatibilized with PP-*g*-MA and EVAL at 2.5–20 wt%, the highest impact strength and elongation at break were obtained at 10 wt% loading. At higher concentrations, performance declined, indicating that excessive compatibilizer disrupted rather than reinforced interfacial adhesion. A similar trend was reported by Raee *et al.*[57] for starch/PP blends modified with PP-*g*-MA, where rheological properties such as storage and loss moduli increased progressively up to 20 wt% compatibilizer. Beyond this level, however, both moduli decreased markedly, attributed to compatibilizer migration into the bulk phases rather than remaining localized at the interface. Consequently, the blend with 30 wt% PP-*g*-MA exhibited the lowest rheological properties. In the same system, elongation at break plateaued at 20 wt% PP-*g*-MA, suggesting saturation of the interfacial region. Collectively, these studies reinforce the present findings: while compatibilizers significantly enhance interfacial adhesion and mechanical properties at optimal concentrations, oversaturation leads to interfacial weakening and processing instabilities.

Further, both optimal formulations produced films with a smooth, uniform surface and sharply reduced melt instabilities. These compatibilizer-rich blends promoted finer dispersion of polyolefin phases, reduced interfacial tension, and enhanced melt elasticity, resulting in more stable flow through the die and firmly holding the polyolefin phases during crystallization. Importantly, the visual improvements in film quality align with the mechanical data trends: optimal formulations not only improved elongation and maintained modulus but also demonstrated more consistent extrusion behavior. While the regression models tended to underpredict ductility, especially in the TD, the qualitative images confirm that formulations with higher EPB and balanced PEMA levels enhance processability and structural uniformity, critical attributes for packaging applications where appearance and performance must both be maintained.

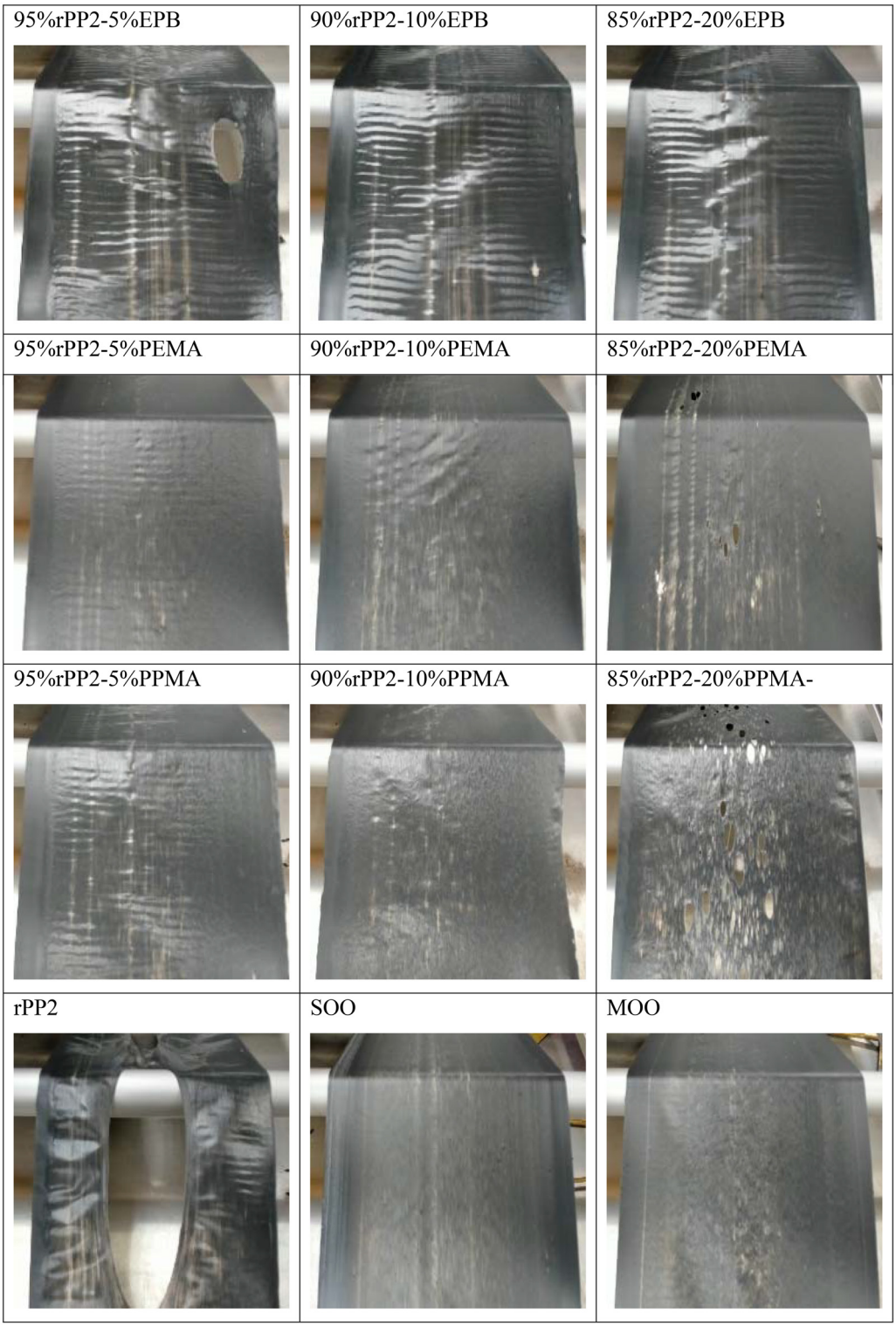

Fig. 2 Film surface appearance during extrusion of rPP2 blends with varying compatibilizer loadings (PEMA, PPMA, EPB), showing the progression from surface irregularities at low levels to smoother, more uniform films near model-predicted optimal formulations.

3.3 Mechanical properties

Multiple regression analyses were performed to quantify the influence of each compatibilizer on three key mechanical responses (elastic modulus, yield strength, and elongation at break), using data from 120 observations obtained from experimental runs 1 through 12. To account for anisotropy introduced during processing, film orientation was encoded in the

model as a categorical factor (MD), where MD = 1 represented specimens tested in the machine (extrusion) direction, and MD = 0 represented specimens tested in the transverse direction (TD).

The regression model revealed significant quadratic terms for PEMA and PPMA, with negative coefficients indicating an adverse relationship. Significant negative quadratic terms for PEMA and PPMA ($p < 0.001$) indicates an optimum yield stress at intermediate loading levels. Estimating an optimal point $x^* = -C_1/2C_2$ where C_1 and C_2 are the linear and quadratic coefficients respectively, the single-factor optima, ignoring interactions, occurred near 0.106 (10.6%) for PEMA and 0.082 (8.2%) for PPMA.‡ This result suggests that yield stress increases with compatibilizer loading up to an optimum point, after which it declines. The likely reason is that excess compatibilizer may lead to phase separation or plasticization effects, detracting from mechanical strength. Interactions between compatibilizers and machine direction (MD) further influenced the modeled yield stress. While the PEMA*PPMA interaction was significantly negative, implying adverse effects when both are combined at certain levels, PPMA*MD interaction was positive and significant, indicating enhanced yield stress along the extrusion direction. This result confirms that processing orientation can modulate the mechanical reinforcement provided by compatibilizers.

Table 2 provides the fitted coefficients and statistics for the regression model for yield stress (R^2 of 0.853). The root mean squared error (RMSE) of 1.51 confirms a good fit between observed and predicted values despite the complex dependence of the yield stress across the rPP blends. The plot comparing the observed and fitted values of yield stress is provided in the SI (Fig. S2). The linear main effects for all three compatibilizers (PEMA, PPMA, and EPB) were positive and statistically significant, demonstrating that each compatibilizer contributes to enhancing the yield stress of the recycled blend. This increase in yield stress is due to some level of interaction between the PP and PE phases of rPP2 with the compatibilizers. In other words, all the compatibilizers tended to improve the interfacial adhesion and stress transfer between polypropylene and polyethylene phases. Notably, PEMA had the largest positive effect, followed by PPMA and EPB.

The model for elongation at break is presented in Table 3 (R^2 of 0.74). The relatively high root mean squared error (RMSE) of 159% strain reflects more significant variability observed in the elongation compared to the yield stress for the tested recycled polymer blends. Inspection of the tested film samples verified greater heterogeneity of the rPP2 matrix in the films comprising polypropylene (~55%), polyethylene (~45%), and minor contaminants such as PET. It is noted that certain terms in the full model exhibit high standard errors (*e.g.* PEMA, PPMA, and EPB). Accordingly, a model sensitivity analysis using backward stepwise elimination of insignificant model terms ($p > 0.50$) yielded a reduced model with effectively similar R^2, RMSE, and model coefficient values. The results of this analysis confirmed that the high standard errors in insignificant terms did not distort the coefficients of the statistically significant factors.

Physically, the main effects of the compatibilizers PEMA, PPMA, and EPB were not statistically significant individually, although PEMA and EPB exhibited positive coefficient estimates, suggesting their potential to enhance ductility. The fitted model coefficients are consistent with the understanding that compatibilizers improve interfacial adhesion and phase dispersion, which can facilitate greater elongation at break. However, elongation showed a pronounced sensitivity to extrusion orientation, as indicated by significant positive interaction terms between compatibilizers and machine direction (MD). Specifically, interactions such as PEMA*MD, PPMA*MD, and EPB*MD were statistically significant ($p < 0.05$). The relatively large coefficients associated with these interaction terms indicate that the effect of each compatibilizer on elongation is strongly influenced by the machine direction (MD); in other words, changes in polymer composition have a much greater impact when the material is oriented along the MD. This reflects the anisotropic nature of the system, where molecular orientation and phase distribution vary with processing direction. Most importantly, however, the large negative model coefficients for PEMA^2*MD and PPMA^2*MD (together with their low p-values confirming statistical significance) imply that the elongation in the transverse direction (TD) is maximized by using moderate values of PEMA and PPMA beyond which elongation may plateau or decrease. The plot comparing the observed and fitted values of elongation at break is provided in the SI (Fig. S3).

Table 4 provides the regression model results for elastic modulus (R^2 of 0.729). The root mean squared error (RMSE) of 69.1 MPa suggests moderate prediction accuracy given mean moduli on the order of 500 MPa. The plot comparing the observed and fitted values of modulus is provided in the SI (Fig. S4). Among the compatibilizers evaluated, only EPB showed a statistically significant positive linear effect on modulus ($p = 0.00086$), indicating a strong reinforcement between the compatibilizer and the matrix (rPP2). The results suggest that increasing EPB content effectively enhances the stiffness of the recycled blend. In contrast, PEMA and PPMA main effects were not significant, indicating their influence on stiffness is less pronounced. This observation is not unexpected, as PEMA and PPMA are inherently soft materials; consequently, their ability to increase modulus is limited and may remain insignificant within the loading range investigated.

Interestingly, machine direction (MD) did not have a significant impact on modulus ($p = 0.46$), which contrasts with its strong influence on elongation and yield stress. This implies that stiffness in recycled PP/PE blends is less sensitive to processing-induced anisotropy, possibly due to the dominant effect of the polymer matrix composition and the reinforcement mechanism imparted by compatibilizers like EPB. The significant negative quadratic term observed for PPMA ($p = 0.0093$) suggests a non-linear relationship with modulus,

‡ For PEMA, $C_1 = \beta_1$ and $C_2 = \beta_9$ while for PPMA, $C_1 = \beta_2$ and $C_2 = \beta_{10}$.

where stiffness increases with PPMA loading up to an optimal point before declining at higher concentrations. This behavior could be attributed to compatibilizer saturation or phase inversion effects that alter the interfacial adhesion and crystallinity within the polymer blend. Another possible explanation is that since PPMA alone is a soft material with low modulus, and at higher concentrations this effect is more significant than morphological modifications due to compatibility. No significant interaction terms involving MD were detected, further supporting the finding that stiffness improvements *via* compatibilization occur largely independent of extrusion direction. Overall, these findings emphasize that EPB is the most effective compatibilizer for enhancing modulus in recycled PP/PE blends, and that stiffness is primarily governed by chemical composition and compatibilizer chemistry rather than processing-induced molecular orientation.

3.4 Optimization result

Overall, the regression models suggest that careful optimization of compatibilizer type, loading level, and anisotropy induced by extrusion direction is critical for maximizing yield strength in recycled PP/PE blends, balancing improved adhesion with the complex morphology inherent to post-consumer recycled blends. As described in the methods section, two optimization strategies were employed: (i) single-objective optimization (SOO) targeting maximum elongation at break in the transverse direction, and (ii) multiple-objective optimization (MOO) balancing the normalized elongation, yield stress, and modulus. For each case, predicted mechanical properties were compared against experimentally observed values in both the machine direction (MD) and transverse direction (TD).

A shown in Table 5, the single-objective optimization aimed at maximizing elongation, particularly in the TD where film stretchability is critical for packaging applications. The model predicted that a formulation of rPP2 (71%), PEMA (9%), PPMA (0%), and EPB (20%) would yield elongations of 1362.90% (MD) and 29.95% (TD), yield stress values of 16.18 MPa (MD) and 11.05 MPa (TD), and moduli of 611.17 MPa (MD) and 626.24 MPa (TD). The experiment results compared to the model predicted results for elongations, were considerably lower in MD (824.10% *vs.* 1363%) but twice greater in TD (66.21% *vs.* 29.95), while stresses at yield (15.63 MPa MD; 7.78 MPa TD) and moduli (625.01 MPa MD; 564.32 MPa TD) showed smaller deviations from predictions. While this confirms the optimization plan targeting elongation in TD, the substantial overestimation of elongation by the model, especially in MD, reflects its sensitivity to the limited dataset and unaccounted influences such as morphological heterogeneity, residual contaminants (*e.g.*, PET), and processing variability. Additionally, the observed TD elongation, which is actually higher than the model predicted value by factor of two, indicates that the anisotropic orientation effects predicted by the model were not as critical under the actual processing and testing conditions. In other words, the material blend formulation for the single objective function G_1 outperformed expectations to maximize elongation in the TD.

For the multiple-objective optimization, the predicted optimal formulation was rPP2 (70%), PEMA (8%), PPMA (2%), and EPB (20%). The model predicted elongations of 1425.33% (MD) and 29.62% (TD), yield stress values of 16.47 MPa (MD) and 10.71 MPa (TD), and moduli of 613.75 MPa (MD) and 621.43 MPa (TD). Experimentally, elongations were again lower in MD (674.05%), but higher in TD (80.36%) while stresses at yield (16.34 MPa MD; 8.39 MPa TD) and moduli (636.05 MPa MD; 534.15 MPa TD) showed better alignment with predictions, particularly for modulus.

While the regression models were not perfect estimators for modulus, yield stress, or elongation to failure, the characterized properties of the optimal blends demonstrate that model-based materials design resulted in higher quality films than expected. The results are of practical significance given the recycled rPP2 blends comprising ~55% PP, ~45% PE, and potential PET or other contaminants where microstructural variability, interfacial adhesion differences, and orientation effects significantly influence ductility. These findings reinforce the importance of experimental verification of

Table 5 Comparison of predicted and experimentally observed mechanical properties for rPP2-based blends at single-objective (maximizing elongation) and multiple-objective (balancing elongation, yield stress, and modulus) optimal formulations. Predicted values are shown on the first line for each property, with corresponding experimental values beneath. MD = machine direction; TD = transverse direction

Optimization	Formulations (%)	Performance measures Observed and experimental outcomes						
		Yield stress (MPa)			Elongation (%)		Modulus (MPa)	
		Type	MD	TD	MD	TD	MD	TD
Single objective optim (elongation at break)	rPP2 = 71, PEMA = 9, PPMA = 0, EPB = 20	Predicted	16.18	11.05	1363	29.95	611.2	626.2
		Observed	15.63	7.781	824.1	66.21	625.01	564.3
Multiple objective optim	rPP2 = 70, PEMA = 8, PPMA = 2, EPB = 20	Predicted	16.47	10.70	1425	29.62	613.8	621.4
		Observed	16.34	8.386	674.05	80.36	636.05	534.2

Baseline	Neat rPP2	Yield stress (MPa)		Elongation (%)		Modulus (MPa)	
		MD	TD	MD	TD	MD	TD
		7.22	1.42	21.26	4.5	459.61	157

model-derived optima, especially for properties sensitive to morphology and processing history.

Fig. 3 compares the predicted and experimentally measured mechanical properties at the model-derived optimal formulations. For both the single-objective and multiple-objective optimizations, modulus predictions closely matched experimental values, while yield stress showed moderate agreement but with a consistent overestimation. Elongation at break exhibited the largest deviations, with the model substantially overpredicting ductility in MD and underpredicting in TD. These discrepancies highlight the model's ability to capture stiffness trends more reliably than ductility-related behavior, likely due to the higher sensitivity of elongation to morphological heterogeneity, contaminants, and processing variability inherent in recycled rPP2 blends.

Fig. 4(a and b) present representative stress–strain curves for all formulations, ranging from low compatibilizer loadings (2.5% PEMA + 2.5% PPMA + 95% rPP2) to the optimized blends. Each curve represents the average response of five tested specimens. The curves highlight the influence of compatibilizer type and concentration on the deformation behavior of rPP2. At low compatibilizer contents, both MD and TD of the blends exhibited relatively brittle behavior with limited elongation, reflecting insufficient interfacial adhesion. Increasing compatibilizer loading, particularly with PEMA and EPB, progressively shifted the curves toward higher elongation and reduced stress concentration, consistent with improved ductility. However, excessive loadings of PEMA or PPMA (20%) led to premature failure and stress softening, supporting the SEM observations of interfacial weakness at high compatibilizer concentrations. In contrast, EPB-containing blends maintained stable deformation up to higher strains, with the 20% EPB formulation displaying the most ductile profile. The optimized blends provided the most balanced performance across MD and TD, combining higher elongation with moderate yield stresses, thereby validating the predictive capability of the regression–optimization framework.

3.5 Microstructure analysis of film samples

The cryofractured surfaces of neat rPP2, compatibilizer-modified blends (5, 10, and 20 wt% of PEMA, PPMA, and EPB), and optimized formulations (single- and multiple-objective) were

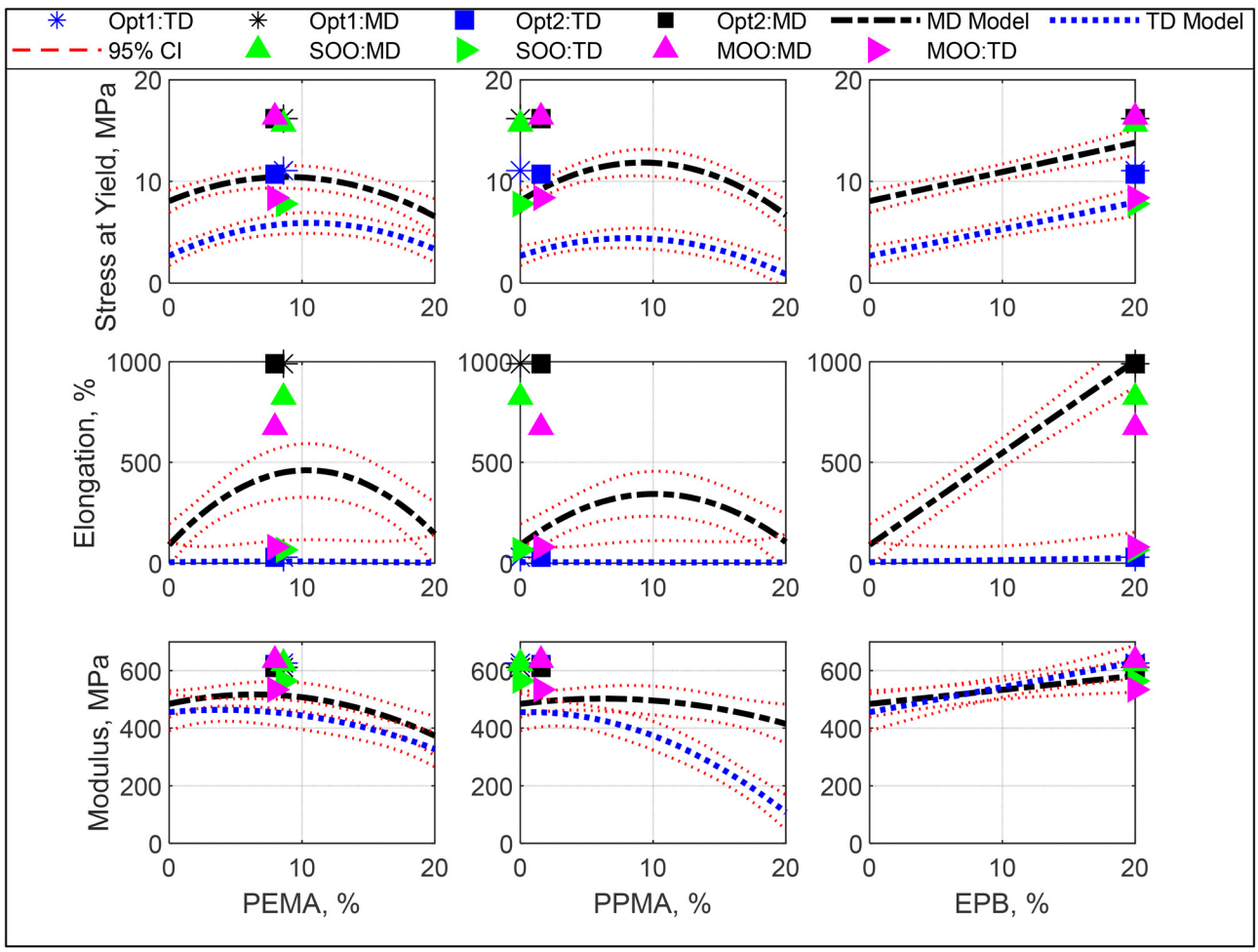

Fig. 3 Comparison of predicted and experimentally measured mechanical properties (yield stress, elongation at break, and modulus) for rPP2 blends at single-objective and multiple-objective optimal formulations in both machine direction (MD) and transverse direction (TD).

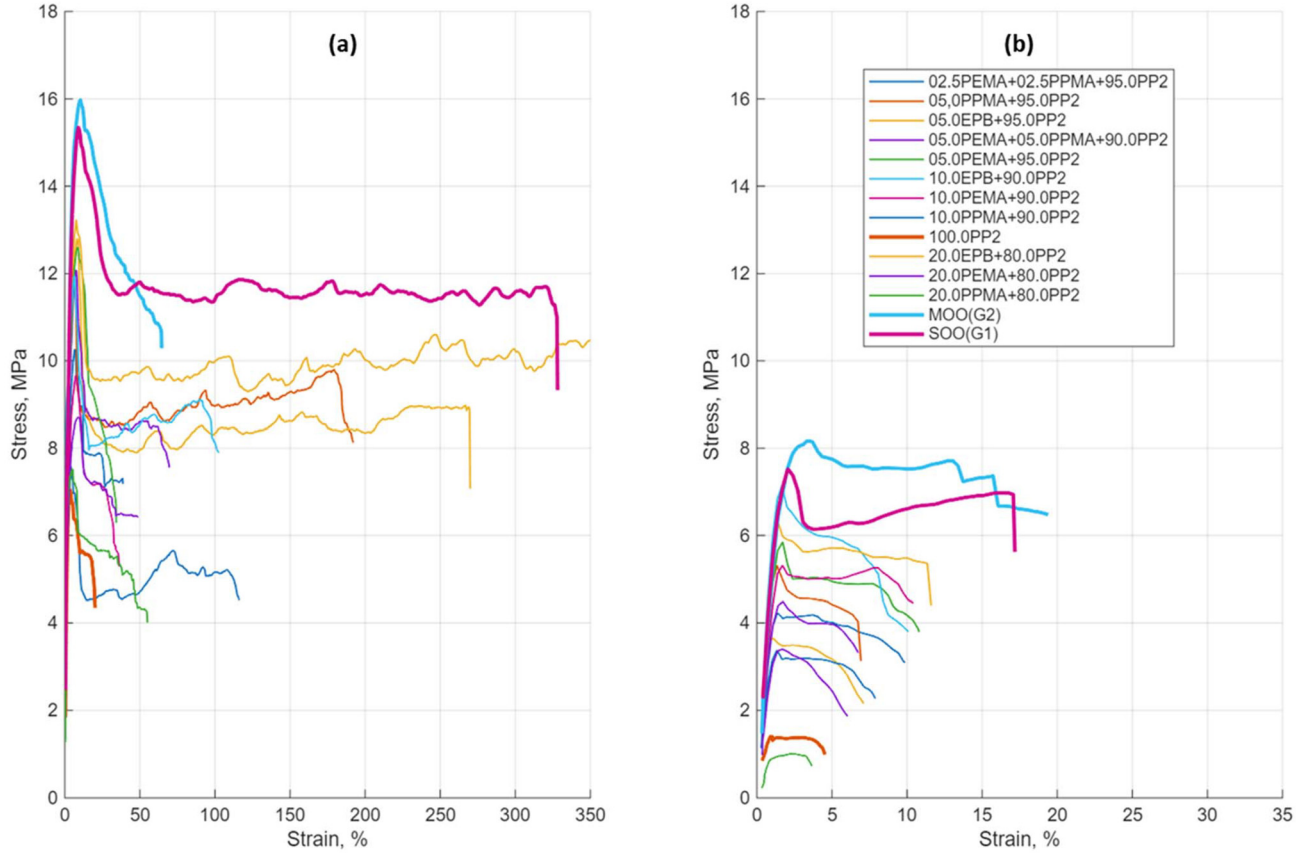

Fig. 4 Representative stress–strain curves of compatibilized rPP2 blends in (a) machine direction (MD) and (b) transverse direction (TD). Each curve represents the average of five specimens. The plots highlight the effect of compatibilizer type and loading on anisotropic deformation behavior.

examined by cross-section taken in the machine direction (MD) using scanning electron microscopy (SEM) to elucidate the effect of compatibilization on phase morphology. As shown in Fig. 5, neat rPP2 exhibits a striated/microfibrillar morphology aligned with MD. As previously characterized,[47] rPP2 consists of ~55% of PP and ~45% HDPE, and these two polyolefin phases form the primary continuous and semi-continuous phases within the recycled matrix. Consistent with prior reports,[58–60] during film extrusion under shear field, the PP/PE phases form striated or microfibrillar morphology. This arises from the immiscibility and sequential crystallization of the two major constituents under shear: PP crystallizes first and is constrained by still-molten PE; PE then crystallizes between PP lamellae, yielding fibrillar striations along MD. It is worth noting that the dispersed spherical void-like features observed in mostly all the samples shown in Fig. 5 are attributed to minor non-polyolefin contaminants, such as polyethylene terephthalate (PET), inherently present in post-consumer recycled rPP2, rather than to the polypropylene or polyethylene phases of the blend.

For PEMA-modified blends, at 5 wt%, striations persist with micro-voids and limited interfacial adhesion, though localized dispersion improves. At 10 wt%, fracture surfaces are more continuous with fewer voids and better lamellar integrity, evidence of enhanced interfacial bonding. At 20 wt%, interfacial separation and more pronounced microfibrillar tearing re-emerge, suggesting over-saturation and phase segregation. These observations are consistent with tensile results: PEMA improves yield stress at low-moderate loadings but shows a negative quadratic effect (optimum at intermediate levels) and limited influence on modulus.

PPMA-modified blends showed a similar trend. At 5 wt%, fibrillar morphology with minor voiding persists. At 10 wt%, parts of the surface appear more homogeneous with reduced fibrillation, indicating improved compatibility. At 20 wt%, void formation and irregular tearing dominate, consistent with reduced processability and interfacial weakening at high loading. This aligns with tensile data showing a negative quadratic term for PPMA (optimum at intermediate loading), a positive PPMA*MD interaction on yield stress, and negligible modulus gains.

The EPB-modified blends exhibited distinct morphologies relative to the maleated compatibilizers. At 5 wt%, the surface is rough and heterogeneous, indicating insufficient bridging. At 10 wt%, micro-voids decrease though MD striations remain apparent. At 20 wt%, striation largely disappears and the surface become smoother with features like agglomerates relating to the ductile fracture of EPB despite being cryogenically

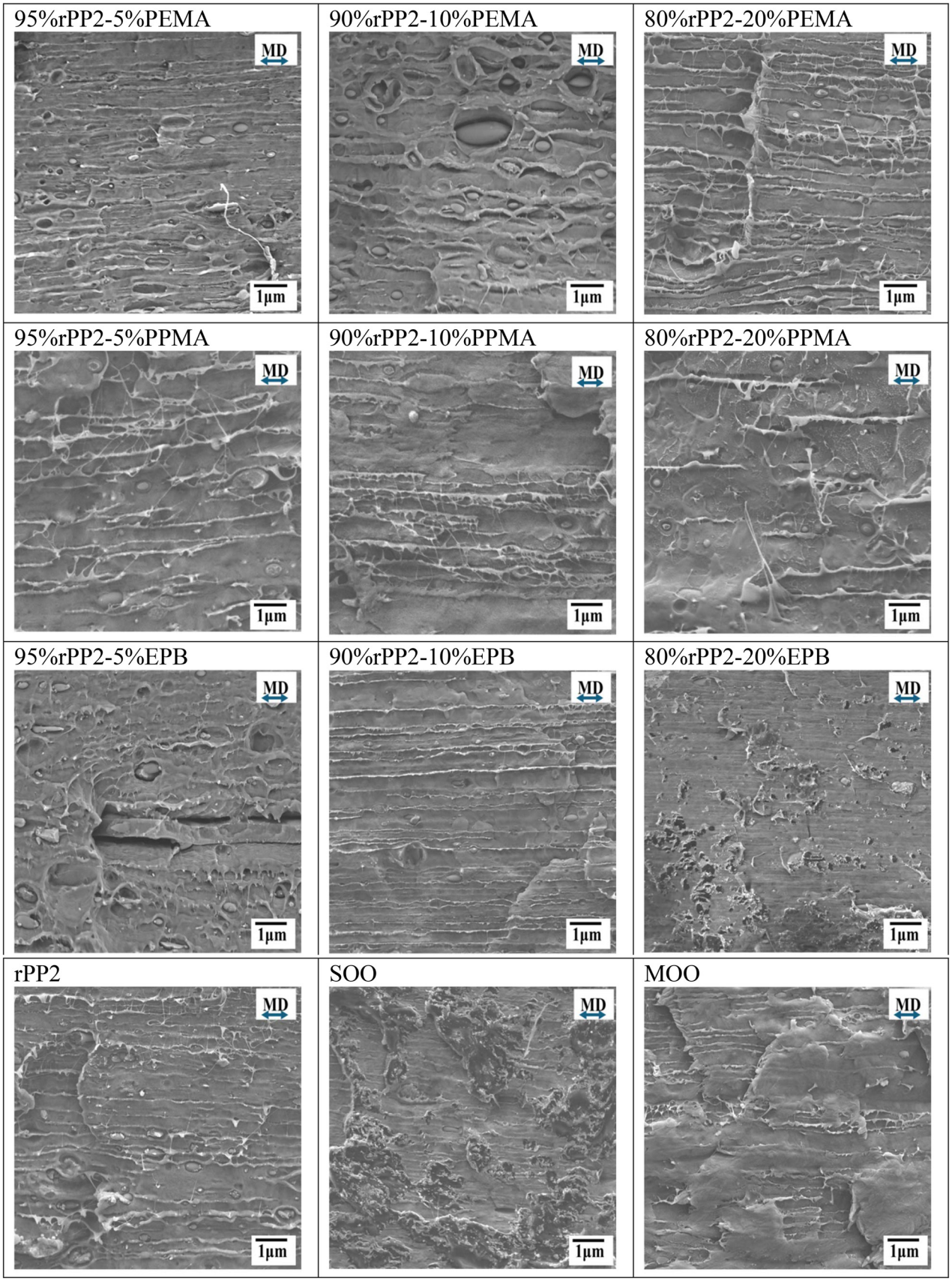

Fig. 5 Cryo-fractured SEM micrographs of neat rPP2, compatibilized blends with PEMA, PPMA, and EPB at 5, 10, and 20 wt% loadings, and single- and multiple-objective optimized samples in the machine direction (MD).

fractured; this is indicative of effective interfacial bridging between PP and PE. This morphological improvement mirrors the mechanical trends: EPB significantly increases modulus, supports stable film extrusion (fewer surface defects), and contributes positively to yield stress.

The single-objective (elongation-targeted) and multiple-objective optima both display more cohesive microstructures than neat rPP2 and most single-component blends. The single-objective sample shows reduced void density and denser lamellar regions interspersed with ductile tearing zones, indicating improved adhesion; however, the dramatic elongation predicted by the model was not realized experimentally, underscoring the influence of residual heterogeneity and processing history. The multiple-objective sample presents the most uniform fracture surface with stronger lamellar continuity and minimal defects, morphology consistent with its balanced mechanical response (robust modulus, reasonable yield stress) and improved processability. This indicates that the small addition of PPMA (2%) in the multiple-objective optimized formulation contributed synergistically with PEMA, providing an additional level of interfacial interaction. This synergy is evident in the processability and SEM morphology, where a smoother film and more continuous fracture surface was observed, and is consistent with the mechanical results, which showed a balanced improvement in both stiffness and ductility. Together, these findings highlight that even minor levels of PPMA can enhance the efficiency of PEMA in compatibilizing the PP/PE phases within rPP2, particularly when combined with EPB at higher loadings.

In summary, SEM corroborates the findings of the mechanical characterization: (i) PEMA and PPMA enhance interfacial adhesion up to ~8–10 wt% but over-loading (20 wt%) promotes interfacial weakness consistent with the observed negative quadratic effects on yield stress; (ii) EPB at 20 wt% effectively bridges PP/PE phases, suppresses striation-driven fracture features, and aligns with the measured stiffness gains and superior film quality; and (iii) optimized blends, especially the multiple-objective formulation, exhibit the most favorable, defect-lean morphologies, validating the compatibilizer strategy while also highlighting the limits of polynomial predictions for elongation in a heterogeneous recycled matrix.

3.6 Microstructural analysis of tensile fracture surfaces

The tensile fracture morphologies of neat rPP2, the single-objective optimized blend, and the multiple-objective optimized blend were examined by SEM in both the machine direction (MD) and transverse direction (TD) to evaluate their failure mechanisms and correlate them with their mechanical performance. As shown in Fig. 6, in the MD, the tensile-fracture surface of neat rPP2 reveals well-aligned lamellae stacked parallel to the tensile axis. This morphology reflects the strong molecular orientation imposed during extrusion and stretching imposed on the self-assembled immiscible PE and PP domains. The absence of significant fibrillation or plastic deformation indicates a brittle-dominated fracture mode, where crack propagation followed the lamellar alignment with minimal resistance. The lamellae acted as planes of weakness, promoting easy crack growth along the interfaces rather than across them, consistent with the low elongation at break of neat rPP2. The TD fracture surface shows a large curled lamellar bundle oriented across the tensile axis. The lamellae appear to peel and delaminate, with weak interlayer adhesion and minimal plastic deformation, again confirming a brittle fracture mechanism. Compared with MD, the TD fracture morphology reflects even greater structural instability, as stress localization forced lamellae to buckle and curl catastrophically. Together, these observations highlight the anisotropic fracture behavior of neat rPP2, with brittle lamellar cleavage in MD and catastrophic lamellar curling and delamination in TD.

For the single-objective optimized formulation, a markedly different fracture morphology was observed. In MD, the surface exhibited rough and irregular features, with clear evidence of torn fibrils, shear information zones, and tearing ridges. These features confirm that the compatibilizer disrupted the lamellar alignment of rPP2, promoting better stress transfer and higher energy absorption. The presence of plastic deformation and fibrillated pull-outs indicates a transition from brittle to ductile fracture, in sharp contrast to neat rPP2. In the TD, the single-objective optimized blend also revealed a rough, irregular morphology with localized shear deformation zones typical of ductile failure. This contrasts strongly with the brittle, lamellar curling seen in neat rPP2, and explains the improved elongation in TD achieved through single-objective optimization, where elongation was specifically targeted.

The fracture morphology of the multiple-objective optimized blend shows further improvements. In MD, the surface is characterized by extensive roughness, fibrillated structures, and highly strained tear ridges, reflecting a ductile-dominated fracture mechanism. The pronounced plastic straining suggests efficient stress redistribution and strong interfacial adhesion between phases, leading to greater energy absorption compared to both neat rPP2 and the single-objective blend. In TD, the fracture surface displays a heterogeneous and extensively deformed morphology, with widespread shear deformation, fibrillar pull-outs, and tearing zones. Unlike neat rPP2, where lamellae delaminated catastrophically, the multiple-objective formulation exhibits progressive plastic failure, indicating that the combination of compatibilizers effectively reduced anisotropy and promoted toughness in both directions.

In summary, the fracture morphology confirms the mechanical trends: neat rPP2 fails in a brittle, anisotropic manner dominated by lamellar cleavage and delamination; the single-objective optimized blend achieves partial ductility, especially in the targeted TD direction; while the multiple-objective optimized blend achieves the most balanced performance, with high ductility, strain tolerance, and energy absorption in both MD and TD.

3.7 Thermal characterization

The melting temperature, T_m (from the second heating cycle) and crystallization temperature, T_c (upon cooling) of rPP2, SOO and MOO were analyzed.

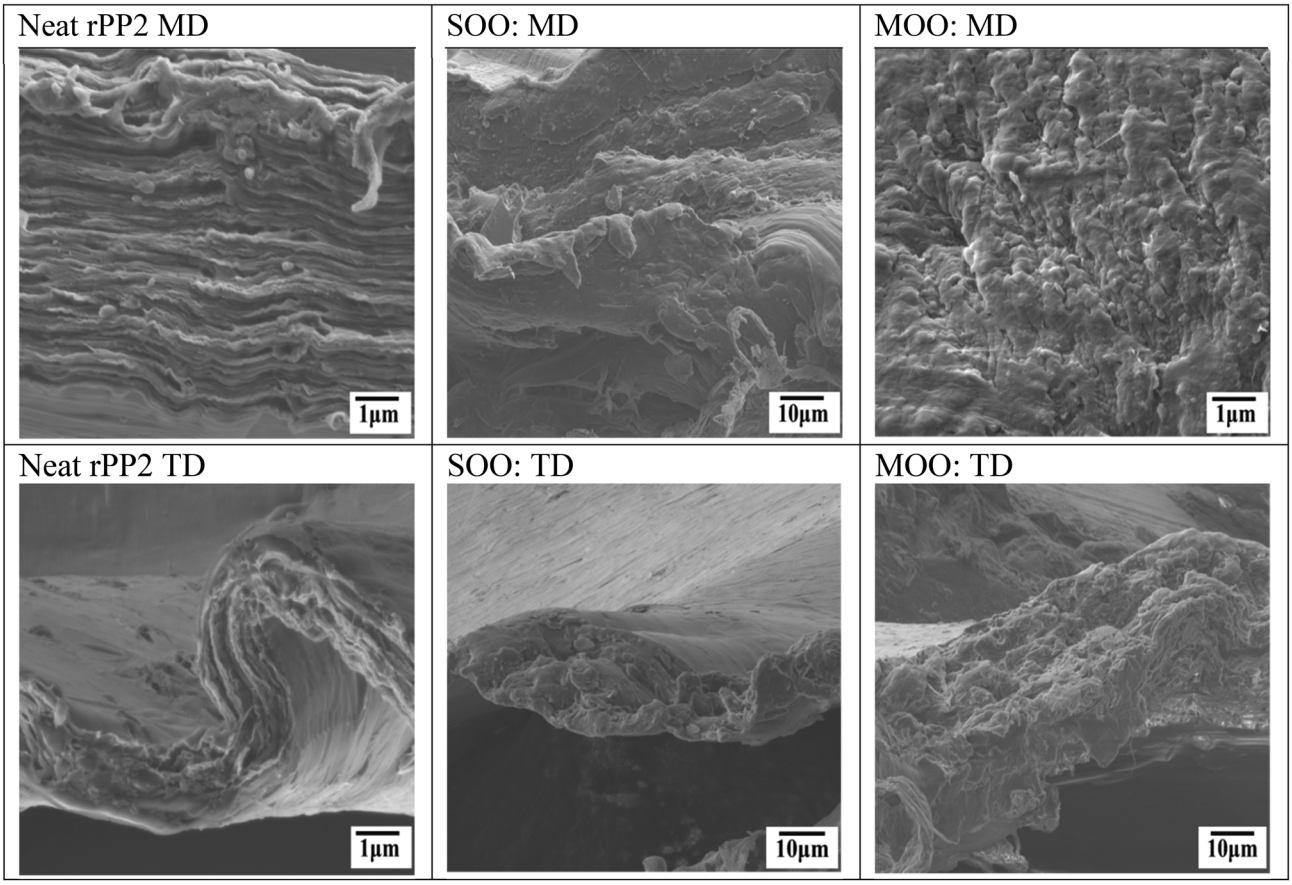

Fig. 6 Micrographs of tensile-fractured surfaces of neat rPP2, single-objective optimized blend, and multiple-objective optimized blend in the machine direction (MD, top row) and transverse direction (TD, bottom row).

Fig. 7 shows the normalized heat flow for the (a) second heating cycle (endothermic up) and (b) the cooling curve (exothermic up). The rPP2 sample exhibited two distinct melting peaks at 130.1 °C and 160.61 °C, corresponding to the melting of the PE and PP domains, respectively, consistent with previous observations in PP/PE blends.[47,61–63]

For the optimized blends (SOO and MOO), the peaks were slightly broader, and the PP phase melting peak shifted to higher temperature (163.11 °C) compared to rPP2, suggesting interactions among rPP2, PEMA, and EPB. While the melting peak of PP phase shifted, the PE phase melting peak was not affected by the incorporation of the compatibilizers. This observation is consistent with the study of F–C. Chiu *et al.*[64] This interaction observed in the SOO and MOO explains the enhanced mechanical performance observed in the optimized samples.

As illustrated in Fig. 7b, in the rPP2 blend, the PP phase starts crystallizing first at a higher temperature (around 121 °C) than the PE phase (118 °C). However, when compatibilizers (PEMA and PPMA) and the elastomer EPB are added in the SOO and MOO samples, they interact with the rPP2 matrix and alter the crystallization kinetics of the PP phase, resulting in the SOO and MOO samples having single T_c peak.

The maleic-anhydride grafted compatibilizers (PEMA and PPMA) partially disrupt the regularity of PP chains and improve interfacial adhesion between PP, PE, and EPB. This likely reduces the mobility of PP chains during cooling, which reduces the crystallization rate of PP and reduces the PP crystallization temperature (T_c). As a result, the PP crystallization peak shifts downward toward lower temperatures and moves closer to the PE crystallization range, causing the peaks to overlap in the SOO and MOO formulations. This observation agrees with findings by Shanks *et al.*,[65] who reported a decrease in the crystallization rate of PP in an LLDPE matrix due to miscibility effects.

Comparing MOO with SOO in both the heating and cooling curves, the addition of 2% PPMA in MOO sharpened the peak of both PE and PP compared to SOO. This sharp peak indicates stronger and enhanced interactions between the PP and EPB phases when little PPMA is present consistent with the tensile results. Although the compatibilizers shifted the PP crystallization peak to lower temperatures due to reduced chain mobility, the corresponding PP melting peak shifted slightly upward. This indicates that the slower crystallization kinetics allowed the formation of thicker and more perfect PP lamellae, resulting in a slight increase in melting temperature despite the reduced T_c.

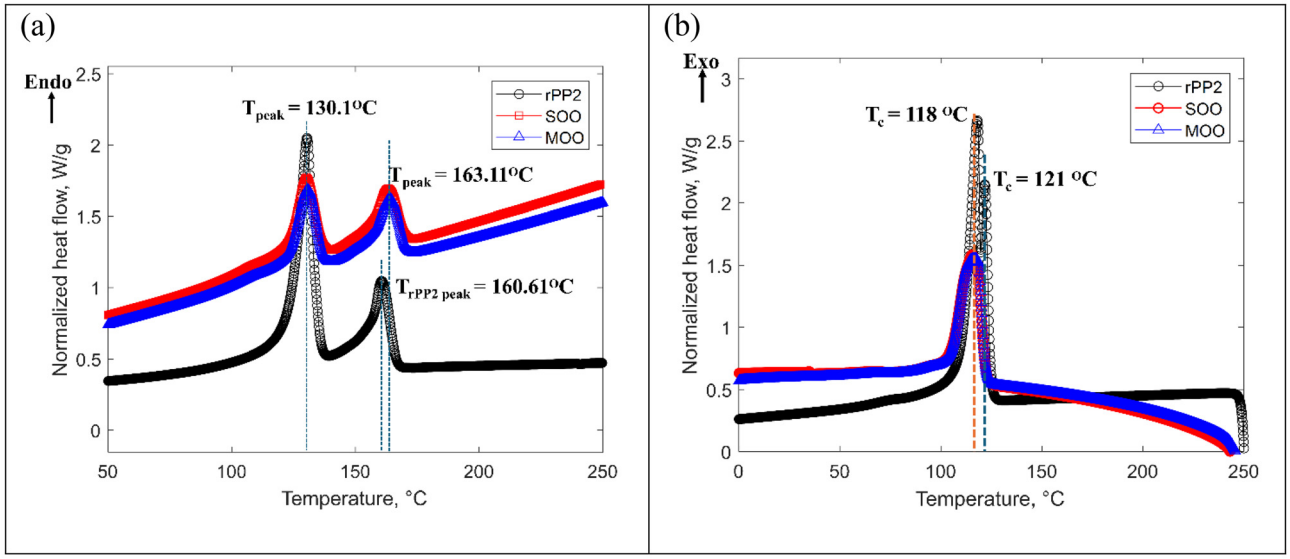

Fig. 7 DSC thermogram (a) second heat cycle (b) cooling curve of rPP2, SOO, and MOO films showing peak shifts and broadening, reflecting enhanced phase compatibility in optimized films.

4. Conclusion

This study systematically evaluated the compatibilization of a post-consumer recycled polypropylene/polyethylene blend (rPP2) using three structurally distinct compatibilizers chosen for their differing mechanisms of action. Maleic anhydride-grafted polyethylene (PEMA) was selected to promote interfacial anchoring to polyethylene-rich domains through free radical grafting, thereby improving stress transfer across otherwise immiscible phases. Maleic anhydride-grafted polypropylene (PPMA), in contrast, provides a complementary mechanism by mixing with polypropylene-rich regions and grafting to the PE phase. Finally, the ethylene–propylene copolymer (EPB) acts through a fundamentally different principle: physical chain entanglement and bridging between PP and PE domains, enhancing phase continuity without relying on chemical reactions. By integrating tensile regression modeling, FTIR spectroscopy, and SEM fracture analysis, the study developed a coherent framework linking these distinct compatibilization strategies to improvements in processability and mechanical performance.

Model-based optimization of the material blends demonstrated that the most effective formulations did not rely on a single compatibilizer, but instead on synergistic combinations that balanced chemical anchoring with physical bridging. Single-objective optimization (maximizing elongation) identified a PEMA–EPB dominated blend that delivered ductility gains, particularly in the transverse direction. Specifically, single-objective optimization (targeting elongation) achieved elongation improvements of ~3776% (MD) and ~1371% (TD) relative to neat rPP2, accompanied by a 36% (MD) and 259% (TD) increase in modulus, and 117% (MD) and 448% (TD) increase in strength. Multiple-objective optimization showed that introducing a minor fraction of PPMA alongside PEMA and EPB produced an even better balance of stiffness, strength, and ductility with strength increased by 126% (MD) and 491% (TD), elongation by 3071% (MD) and 1686% (TD), and stiffness by 38% (MD) and 240% (TD). This synergy highlights the importance of tailoring compatibilizer strategies not only to individual property enhancements but also to the combined mechanical performance required for high-value applications.

Although the primary focus of this study was on mechanical properties, previous rheological analyses of rPP2 (capillary and parallel-plate rheology) provide insights into its flow behavior.[47] The results indicate that rPP2 possesses sufficient melt viscosity for film extrusion. However, extrusion experiments revealed instabilities such as melt fracture and film bifurcation, which are attributed to the high proportion of incompatible PP and PE phases. These findings suggest that while rheology can inform processing parameters, it does not fully capture the effects of phase incompatibility on extrusion behavior. Further rheological investigations could provide deeper understanding of these instabilities and guide optimization of compatibilization strategies.

In conclusion, this study demonstrates that material characterization and compatibilization strategies tailored to balance physical and interfacial interactions can mitigate the heterogeneity of post-consumer recycled polyolefins. By integrating FTIR, SEM, regression modeling, and optimization, we establish a viable pathway to improve processability, toughness, and stiffness simultaneously. Considering the PP/PE composition of rPP2 (55/45), the compatibilizers examined in this study represent the principal and practically relevant compatibilization strategies available for PP/PE systems: PP-based reactive compatibilization (PP-*g*-MA), PE-based reactive compatibilization

(LLDPE-*g*-MA), and non-reactive architecture-driven compatibilization *via* a PE-PP copolymer. Practically, the findings of this study support the use of compatibilized rPP2 and similarly varied materials in higher-value packaging, film, and structural applications, where ductility, strength, and stiffness must be carefully balanced. This contributes to advancing the circular economy of plastics, enabling broader adoption of recycled polyolefins in technically demanding applications.

Conflicts of interest

There are no conflicts to declare.

Data availability

Data for this article, including comma separated values for the mechanical testing data, Matlab codes, SEM images, process film images and FTIR spectra are available at https://doi.org/10.34863/x11r-nk70.

Supplementary information (SI) is available. See DOI: https://doi.org/10.1039/d5lp00321k.

Acknowledgements

This work is supported by the National Science Foundation (NSF) under Grant No. 2118808, DMREF/Collaborative Research: Integrated Material Design and Processing—Application to Recycled Plastics (12/01/2021–11/30/2025). Any opinions, findings, conclusions, or recommendations expressed in this material are those of the authors and do not necessarily reflect the views of the NSF. The authors also wish to thank Geon Performance Solutions (Avon Lake, OH) for generously providing the recycled materials used in this study.

References

1 G. V. Research, *Polyolefin Market Size, Share & Trends Analysis Report By Product (PE, PP, EVA, TPO, POM, PC, PMMA), By Application (Film & Sheet, Injection Molding, Blow Molding, Profile Extrusion), By Region, And Segment Forecasts, 2025–2030*, 2024, pp. 1–15. https://www.grandviewresearch.com/industry-analysis/polyolefin-market# [accessed July, 2025].

2 G. V. Research, *Polypropylene Market Size, Share & Trends Analysis Report By Polymer Type (Homopolymer, Copolymer), By Process, By Application, By End-Use, By Region, And Segment Forecasts, 2023–2030*, Grand View Research, 2022, pp. 1–10. https://www.grandviewresearch.com/industry-analysis/polypropylene-market#:~:text=The%20global%20polypropylene%20market%20size,packaging%2C%20and%20building%20&%20construction [accessed July, 2025].

3 G. V. Research, *Polyethylene Market Size, Share & Trends Analysis Report By Product (LDPE, HDPE), By Application (Bottles & Containers, Films & Sheets), By End-use, By Region, And Segment Forecasts, 2024–2030*, Grand View Research, 2022, pp. 1–10. https://www.grandviewresearch.com/industry-analysis/polyethylene-pe-market#:~:text=The%20global%20polyethylene%20market%20size,growth%20over%20the%20forecast%20period [accessed July, 2025].

4 R. Geyer, J. R. Jambeck and K. L. Law, Production, use, and fate of all plastics ever made, *Sci. Adv.*, 2017, **3**(7), e1700782, DOI: 10.1126/sciadv.1700782.

5 Waste360, *Plastics Packaging Recyclers Attribute Low Recycling Rates to Lacking Collections*, Waste360, 2022, pp. 1–5. https://www.waste360.com/plastics/plastics-packaging-recyclers-attribute-low-recycling-rates-to-lacking-collections. [Accessed July, 2025].

6 P. Bovee, *Why is Polypropylene (PP) So Difficult to Recycle?, Report*, Cleantech Insights, Waste & Recycling, 2024, 1. https://www.cleantech.com/why-is-polypropylene-pp-so-difficult-to-recycle/ [accessed July, 2025].

7 A. Polyportis, L. Magnier and R. Mugge, Guidelines to Foster Consumer Acceptance of Products Made from Recycled Plastics, *Circ. Econ. Sustainability*, 2023, **3**(2), 939–952, DOI: 10.1007/s43615-022-00202-9.

8 J. Shi and Z. Jiang, Willingness to pay a premium price for green products: does a reference group matter?, *Environ., Dev. Sustainability*, 2023, **25**(8), 8699–8727, DOI: 10.1007/s10668-022-02419-y.

9 D. Achilias, E. Antonakou, C. Roupakias, P. Megalokonomos and A. Lappas, Recycling techniques of polyolefins from plastic wastes, *Global NEST J.*, 2008, **10**(1), 114–122.

10 K. Faust, P. Denifl and M. Hapke, Recent advances in catalytic chemical recycling of polyolefins, *ChemCatChem*, 2023, **15**(13), e202300310, DOI: 10.1002/cctc.202300310.

11 S. Kumar, A. K. Panda and R. K. Singh, A review on tertiary recycling of high-density polyethylene to fuel, *Resour., Conserv. Recycl.*, 2011, **55**(11), 893–910, DOI: 10.1016/j.resconrec.2011.05.005.

12 L. Utracki, Reprocessing of Commingled Polymers and Recycling of Polymer Blends, in *Frontiers in the Science and Technology of Polymer Recycling*, Springer, 1998, pp. 333–354.

13 K. Kaiser, M. Schmid and M. Schlummer, Recycling of polymer-based multilayer packaging: A review, *Recycling*, 2017, **3**(1), 1, DOI: 10.3390/recycling3010001.

14 A. Creations, MatWeb: Online Materials Information Resource. Internet. https://www.matweb.com/search [accessed July, 2025].

15 J. Teh, A. Rudin and J. C. Keung, A review of polyethylene–polypropylene blends and their compatibilization, *Adv. Polym. Technol.*, 1994, **13**(1), 1–23, DOI: 10.1002/adv.1994.060130101.

16 J. Teh, Structure and properties of polyethylene–polypropylene blend, *J. Appl. Polym. Sci.*, 1983, **28**(2), 605–618, DOI: 10.1002/app.1983.070280216.

17 S. Krause, *Polymer Blends*, ed. D. R. Paul and S. Newman, Academic Press New York, 1978.

18 K. Šolc, Polymer Compatibility and Incompatibility: Principles and Practices: Papers Presented at the Tenth Midland Macromolecular Meeting, Held August 18–22, 1980 in Midland, Michigan, Taylor & Francis, 1982.
19 Y. Kazemi, A. Ramezani Kakroodi and D. Rodrigue, Compatibilization efficiency in post–consumer recycled polyethylene/polypropylene blends: Effect of contamination, *Polym. Eng. Sci.*, 2015, **55**(10), 2368–2376, DOI: 10.1002/pen.24125.
20 S. Serranti, V. Luciani, G. Bonifazi, B. Hu and P. C. Rem, An innovative recycling process to obtain pure polyethylene and polypropylene from household waste, *Waste Manage.*, 2015, **35**, 12–20, DOI: 10.1016/j.wasman.2014.10.017.
21 S. Yin, R. Tuladhar, F. Shi, R. A. Shanks, M. Combe and T. Collister, Mechanical reprocessing of polyolefin waste: A review, *Polym. Eng. Sci.*, 2015, **55**(12), 2899–2909, DOI: 10.1002/pen.24182.
22 M. Messiha, A. Frank, T. Koch, F. Arbeiter and G. Pinter, Effect of polyethylene and polypropylene cross-contamination on slow crack growth resistance, *Int. J. Polym. Anal. Charact.*, 2020, **25**(8), 649–666, DOI: 10.1080/1023666X.2020.1833143.
23 P. Pötschke and D. R. Paul, Formation of Co-continuous Structures in Melt-Mixed Immiscible Polymer Blends, *J. Macromol. Sci., Part C*, 2003, **43**(1), 87–141, DOI: 10.1081/MC-120018022.
24 M. Kozderka, B. Rose, N. Bahlouli, V. Kočí and E. Caillaud, Recycled high impact polypropylene in the automotive industry - mechanical and environmental properties, *Int. J. Interact. Des. Manuf.*, 2017, **11**(3), 737–750, DOI: 10.1007/s12008-016-0365-9.
25 J. Teh, H. Blom and A. Rudin, A study on the crystallization behaviour of polypropylene, polyethylene and their blends by dynamic mechanical and thermal methods, *Polymer*, 1994, **35**(8), 1680–1687, DOI: 10.1016/0032-3861(94)90842-7.
26 D. E. Huang, A. P. Kotula, C. R. Snyder and K. B. Migler, Crystallization kinetics in an immiscible polyolefin Blend, *Macromolecules*, 2022, **55**(24), 10921–10932, DOI: 10.1021/acs.macromol.2c01691.
27 N.-D. Tien and R. E. Prud'homme, Crystallization behavior of semicrystalline immiscible polymer blends, in *Crystallization in Multiphase Polymer Systems*, Elsevier, 2018, pp. 181–212.
28 X. Lin, Y. Liu, X. Chen, *et al.*, Reactive compatibilization of polyamide 6/olefin block copolymer blends: phase morphology, rheological behavior, thermal behavior, and mechanical properties, *Materials*, 2020, **13**(5), 1146, DOI: 10.3390/ma13051146.
29 L. D'orazio, R. Greco, E. Martuscelli and G. Ragosta, Effect of the addition of EPM copolymers on the properties of high density polyethylene/isotactic polypropylene blends: II. Morphology and mechanical properties of extruded samples, *Polym. Eng. Sci.*, 1983, **23**(9), 489–497.
30 V. Choudhary, H. Varma and I. Varma, Effect of EPDM rubber on melt rheology, morphology and mechanical properties of polypropylene/HDPE (9010) blend. 2, *Polymer*, 1991, **32**(14), 2541–2545, DOI: 10.1016/0032-3861(91)90333-E.
31 J. Song, A. Bringuier, S. Kobayashi, A. M. Baker and C. W. Macosko, Adhesion between polyethylenes and different types of polypropylenes, *Polym. J.*, 2012, **44**(9), 939–945, DOI: 10.1038/pj.2012.25.
32 Y. Lin, G. R. Marchand, A. Hiltner and E. Baer, Adhesion of olefin block copolymers to polypropylene and high density polyethylene and their effectiveness as compatibilizers in blends, *Polymer*, 2011, **52**(7), 1635–1644, DOI: 10.1016/j.polymer.2011.02.012.
33 V. Flaris, A. Wasiak and W. Wenig, The effect of compatibilizers on the morphology of isotactic polypropylene/linear low-density polyethylene blends, *J. Mater. Sci.*, 1993, **28**(6), 1685–1688, DOI: 10.1007/BF00363368.
34 C. Kock, N. Aust, C. Grein and M. Gahleitner, Polypropylene/polyethylene blends as models for high–impact propylene–ethylene copolymers, part 2: Relation between composition and mechanical performance, *J. Appl. Polym. Sci.*, 2013, **130**(1), 287–296, DOI: 10.1002/app.39181.
35 S. Vervoort, J. Den Doelder, E. Tocha, *et al.*, Compatibilization of polypropylene–polyethylene blends, *Polym. Eng. Sci.*, 2018, **58**(4), 460–465, DOI: 10.1002/pen.24661.
36 C. Marco, G. Ellis, M. Gómez, *et al.*, Rheological properties, crystallization, and morphology of compatibilized blends of isotactic polypropylene and polyamide, *J. Appl. Polym. Sci.*, 1997, **65**(13), 2665–2677.
37 A. Graziano, S. Jaffer and M. Sain, Review on modification strategies of polyethylene/polypropylene immiscible thermoplastic polymer blends for enhancing their mechanical behavior, *J. Elastomers Plastics*, 2018, **51**(4), 291–336, DOI: 10.1177/0095244318783806.
38 C. Tselios, D. Bikiaris, V. Maslis and C. Panayiotou, In situ compatibilization of polypropylene–polyethylene blends: a thermomechanical and spectroscopic study, *Polymer*, 1998, **39**(26), 6807–6817, DOI: 10.1016/S0032-3861(98)00132-3.
39 A. Colbeaux, F. Fenouillot, J. F. Gérard, M. Taha and H. Wautier, Compatibilization of a polyolefin blend through covalent and ionic coupling of grafted polypropylene and polyethylene. I. Rheological, thermal, and mechanical properties, *J. Appl. Polym. Sci.*, 2005, **95**(2), 312–320, DOI: 10.1002/app.21226.
40 A. Graziano, O. A. Titton Dias, B. Sena Maia and J. Li, Enhancing the mechanical, morphological, and rheological behavior of polyethylene/polypropylene blends with maleic anhydride–grafted polyethylene, *Polym. Eng. Sci.*, 2021, **61**(10), 2487–2495, DOI: 10.1002/pen.25775.
41 W. Shao, L. Liu, Y. Wang, X. Hua, F. Zhang and Y. Shi, Crystallization, structure, and properties of polypropylene random copolymer (PPR)/high-density polyethylene/polypropylene grafted maleic anhydride((HDPE/PP)-g-MAH) blends, *J. Polym. Res.*, 2022, **29**(8), 354, DOI: 10.1007/s10965-022-03211-2.
42 F. Ide and A. Hasegawa, Studies on polymer blend of nylon 6 and polypropylene or nylon 6 and polystyrene using the

reaction of polymer, *J. Appl. Polym. Sci.*, 1974, **18**(4), 963–974, DOI: 10.1002/app.1974.070180402.

43 A. González-Montiel, H. Keskkula and D. Paul, Morphology of nylon 6/polypropylene blends compatibilized with maleated polypropylene, *J. Polym. Sci., Part B: Polym. Phys.*, 1995, **33**(12), 1751–1767, DOI: 10.1002/polb.1995.090331206.

44 A. Tedesco, R. Barbosa, S. Nachtigall and R. Mauler, Comparative study of PP-MA and PP-GMA as compatibilizing agents on polypropylene/nylon 6 blends, *Polym. Test.*, 2002, **21**(1), 11–15, DOI: 10.1016/S0142-9418(01)00038-1.

45 K. H. Yoon, H. W. Lee and O. O. Park, Properties of poly(ethylene terephthalate) and maleic anhydride–grafted polypropylene blends by reactive processing, *J. Appl. Polym. Sci.*, 1998, **70**(2), 389–395, DOI: 10.1002/(SICI)1097-4628(19981003)70:2%3C389::AID-APP20%3E3.0.CO;2-Z.

46 M. Xu, J. Liao, Z. Luo, *et al.*, Study of polypropylene/polyethylene terephthalate blends compatibilized with polypropylene double–grafted maleic anhydride and epoxy resin, *J. Appl. Polym. Sci.*, 2024, **141**(42), e56117, DOI: 10.1002/app.56117.

47 D. O. Kazmer, S. O. Nzeh, B. Shen, *et al.*, Characterization, processing, and modeling of industrial recycled polyolefins, *Polym. Eng. Sci.*, 2024, **64**(10), 4801–4815, DOI: 10.1002/pen.26882.

48 N. Abacha and S. Fellahi, Synthesis of polypropylene–graft–maleic anhydride compatibilizer and evaluation of nylon 6/polypropylene blend properties, *Polym. Int.*, 2005, **54**(6), 909–916, DOI: 10.1002/pi.1788.

49 A. Colbeaux, F. Fenouillot, J. F. Gerard, M. Taha and H. Wautier, Compatibilization of a polyolefin blend through covalent and ionic coupling of grafted polypropylene and polyethylene. II. Morphology, *J. Appl. Polym. Sci.*, 2004, **93**(5), 2237–2244, DOI: 10.1002/app.21226.

50 L. D'orazio, R. Greco, C. Mancarella, E. Martuscelli, G. Ragosta and C. Silvesrte, Effect of the addition of ethylene–propylene random copolymers on the properties of high–density polyethylene/isotactic polypropylene blends: Part 1—morphology and impact behavior of molded samples, *Polym. Eng. Sci.*, 1982, **22**(9), 536–544, DOI: 10.1002/pen.760220904.

51 ASTM D882-18, *Standard Test Method for Tensile Properties of Thin Plastic Sheeting*, ASTM International, West Conshohocken, PA, 2018; https://store.astm.org/d0882-18.html.

52 F. Gu, P. Hall, N. J. Miles, Q. Ding and T. Wu, Improvement of mechanical properties of recycled plastic blends via optimizing processing parameters using the Taguchi method and principal component analysis, *Mater. Des.*, 2014, **62**, 189–198, DOI: 10.1016/j.matdes.2014.05.013.

53 D. Kazmer and C. Roser, Evaluation of Product and Process Design Robustness, *Res. Eng. Des.*, 1999, **11**(1), 20–30, DOI: 10.1007/s001630050002.

54 Y. Zhang, Solving large-scale linear programs by interior-point methods under the Matlab * Environment †, *Optim. Methods Softw.*, 1998, **10**(1), 1–31, DOI: 10.1080/10556789808805699.

55 S. T. Nicolau and A. J. Matzger, An evaluation of resolution, accuracy, and precision in FT-IR spectroscopy, *Spectrochim. Acta, Part A*, 2024, **319**, 124545, DOI: 10.1016/j.saa.2024.124545.

56 A. B. D. Nandiyanto, R. Oktiani and R. Ragadhita, How to read and interpret FTIR spectroscope of organic material, *Indones. J. Sci. Technol.*, 2019, **4**(1), 97–118, DOI: 10.17509/ijost.v4i1.15806.

57 E. Raee, A. Avid and B. Kaffashi, Effect of compatibilizer concentration on dynamic rheological behavior and morphology of thermoplastic starch/polypropylene blends, *J. Appl. Polym. Sci.*, 2020, **137**(22), 48742, DOI: 10.1002/app.48742.

58 S. O. Nzeh, D. O. Kazmer and M. J. SobkowiczKline, Mitigating Extrusion Instabilities and Enhancing Mechanical Performance of Post–Consumer Recycled Polyolefins via Layer Multiplying Elements, *Polym. Eng. Sci.*, 2025, **1**, 1–18, DOI: 10.1002/pen.70105.

59 M. Polaskova, R. Cermak, T. Sedlacek, J. Kalus, M. Obadal and P. Saha, Extrusion of polyethylene/polypropylene blends with microfibrillar–phase morphology, *Polym. Compos.*, 2010, **31**(8), 1427–1433, DOI: 10.1002/pc.20928.

60 J. Výchopňová, R. Čermák and M. Obadal, Morphology variations of polypropylene, in *Modern Research and Educational Topics in Microscopy*, 2007, pp. 704–712.

61 A. C. Y. Wong and F. Lam, Study of selected thermal characteristics of polypropylene/polyethylene binary blends using DSC and TGA, *Polym. Test.*, 2002, **21**(6), 691–696, DOI: 10.1016/S0142-9418(01)00144-1.

62 L. Delva, L. Cardon and K. Ragaert, Evaluation of post-consumer mixed polyolefines and their injection moulded blends with virgin polyethylene, *Environ. Eng. Manage. J.*, 2018, **17**(2), 430–432.

63 S. Hubo, L. Leite, C. Martins and K. Ragaert, *Evaluation of post-industrial and post-consumer polyolefin-based polymer waste streams for injection moulding*. 2014, pp. 201–206.

64 F.-C. Chiu, H.-Z. Yen and C.-E. Lee, Characterization of PP/HDPE blend-based nanocomposites using different maleated polyolefins as compatibilizers, *Polym. Test.*, 2010, **29**(3), 397–406, DOI: 10.1016/j.polymertesting.2010.01.004.

65 R. A. Shanks, J. Li and L. Yu, Polypropylene–polyethylene blend morphology controlled by time–temperature–miscibility, *Polymer*, 2000, **41**(6), 2133–2139, DOI: 10.1016/S0032-3861(99)00399-7.